PERGAMON

Vision Research 38 (1992) 1843–1859

Vision Research

Evidence for spatial aliasing effects in the Y-like cells of the magnocellular visual pathway

T. Maddess [a,*], J.M. Hemmi [b], A.C. James [b]

[a] *Visual Sciences, Research School of Biological Sciences, Australian National University, Canberra ACT 0200, Australia*
[b] *Developmental Neurobiology, Research School of Biological Sciences, Australian National University, Canberra ACT 0200, Australia*

Received 22 July 1996; received in revised form 24 September 1997

Abstract

Several lines of evidence are provided indicating that our visual percept can be dominated by spatial aliasing for viewing conditions near those needed to see the spatial frequency doubled illusion. The apparent aliasing effect indicates that the underlying sampling array has a density 15–30% of that of M-cells, in agreement with the known proportion of Y-like M-cells (M_y-cells). The presence of aliasing indicates, that there is a separate irregular array of M_y-cells, and that their role is to rapidly convey information on retinal gain control to the brain rather than to act primarily as inputs to image motion computation.

Keywords: Aliasing; Adaptation; Illusion; Motion; Y-cell

1. Introduction

The experiments described here attempt to examine the angular separation between the units responsible for the spatial frequency doubled (FD) illusion [1]. Subjects see the FD illusion when they view low spatial frequencies whose contrast is modulated in time at high temporal frequencies. Under these conditions subjects report seeing grating patterns with twice as many cycles as in the original pattern. Tyler [2], suggested that the illusion arose from retinal ganglion cells with rectifying responses to contrast modulation. Cat Y-cells [3] and their primate analogues the Y-like cells of the magnocellular pathway (M_y-cells) [4], have a strong full wave rectified response component. Studies of cat Y-cells [5,6] indicate that the rectifier's response is proportional to the absolute value of the stimulus contrast raised to an exponent of 0.7–0.8, e.g. $\sim |c|^{0.7}$. The nonlinearity responsible for the FD illusion has the same form [7].

Further evidence for a retinal origin for the FD illusion comes from the observation that the ability of persons with glaucoma to see the FD illusion is severely impaired [8–14]. Results from these methods are highly correlated with Pattern electroretinograms (PERGs) obtained with FD stimuli [13], and with the results of automated perimetry. Sensitivities and specificities around 97% for diagnosing early glaucomas have been confirmed [14]. The accuracy of these methods may point to M_y-cells as the source of the FD illusion because M_y-cells appear to be the largest of the retinal ganglion cells, larger even than the M_x-cells [15–17] and retinal ganglion cells appear to die-off in proportion to their soma size in glaucoma [18–21]. Larger cells in the parvicellular pathway are also killed at higher rates [21] which may account for strong deficits in blue/yellow system observed in glaucoma [22].

Much of our knowledge of primate retinal ganglion cells is drawn from studies of macaques. The visual acuity and contrast sensitivity of Macaques is similar to humans [23–25] and the distribution of ganglion cells in the Macaque retina appears to be very similar to that of the human [26–28]. Anatomical studies on Macaques indicate that 10% of the retinal ganglion cells projecting to the LGN terminate in the Magnocellular layers [29]. Electrophysiological studies reveal that 5–25% of the LGN M-cells [17,15,16,30] show the response signature of cat Y-cells. The responses of the LGN cells appear to mirror that of their presynaptic retinal ganglion cells [31–34]. The combined anatomi-

* Corresponding author. Tel.: +61 2 62494099; fax: +61 2 62493808; e-mail: Ted.Maddess@anu.edu.au.

0042-6989/98/$19.00
PII: S0042-6989(97)00344-1

cal and physiological data indicate that the Magnocellular Y-cells or 'M_y-cells' represent only about 1–2% of all retinal ganglion cells. All the evidence suggests that humans would have a similar fraction of M_y-cells.

But what is it about M_y-cell physiology that might make the FD illusion visible only at low spatial and high temporal frequencies? The answer may be the retinal gain control of Shapley and Victor [35], which is strongly expressed in primate M-cells [30,36] but not in P-cells. With the correct visual stimuli this gain control is switched on providing large nonlinear responses [35,37,38]. Under conditions of low spatial and high temporal frequencies Y-cell second harmonic responses, indicative of rectification, can be ten times the linear response [5,39]. Responses of P cells are not affected by gain control [36], and both P-cells and the other subclass of M cells (M_x), are quite linear, reducing their potential as sources of second harmonic responses. Recent PERG studies indicate that when conditions for seeing the FD illusion are approached, the PERG signal [40–42] becomes dominated by responses showing phase shifts indicative of the action of retinal gain control upon the second harmonic responses of Y-type cells [39].

If the units responsible for the illusion are the M_y-cells then the angular separation between these cells should be accessible given that the sampling array of M_y-cells should suffer from spatial aliasing. Aliasing arises when the density of an array of samplers is insufficient to reconstruct the highest spatial frequency detected by an individual sampler. This critical sampling limit, often called the Nyquist frequency, will be referred to here as the critical spatial frequency (S_c). Excellent discussions of sampling theory [43,44] and its application to spatial vision e.g. [45–51] are available. Of particular relevance to this study is the work of Coletta *et al.* [52] and Galvin *et al.* [53].

The coverage factor (the number of cells seeing each point in visual space due to receptive field overlap) of M-cells has been estimated anatomically [54,55] and electrophysiologically [32] to lie between two and seven. If M_y-cells represent only 10% of all M ganglion cells then their coverage factor would be in the range 0.2–0.7. This means that the array of M_y-cells would seriously undersample the image and suffer from aliasing effects (see below) because individual cells would encode information about spatial frequencies which could not be encoded veridically given the low density of their array. By inspection of the available data [17] the highest spatial frequency the individual M_y-cells can respond to appears to be about four to eight times higher than the Nyquist frequency imposed by their low density. Thus if M_y-cell activity could be unmasked by some particular class of visual stimuli one would expect to see the effects of spatial undersampling. Spatial aliasing effects attributable to retinal ganglion cells have been observed in peripheral vision [56–59] but see [60]. One of the most interesting of these effects is what is known as motion reversal. Motion reversal attributed to postreceptoral processes has also been reported [61] and this has recently been attributed to the parvicellular pathway indicating that this array determines the upper spatial limit on motion acuity [62,59,53].

For a 1 dimensional set of periodic detectors a moving sinusoidal intensity grating with spatial frequency S in the range $S_c < S < 2S_c$, will be seen as a lower spatial frequency ($2S_c - S$) alias pattern moving in the opposite direction to its actual movement. For an orderly two dimensional array of detectors the direction of motion will appear to be opposite to actual motion only near the cut-off frequency S_c (see [43,47] for discussion of S_c for higher dimensional sampling) and will otherwise been seen at other orientations [63]. In a disorderly array the alias is a noisy pattern, band limited in spatial frequency and orientation, typically moving in the opposite direction to the veridical direction [52].

Motion reversal for the case of sampling with a realistic irregular array can be understood by examining Fig. 1. The spectrum of a disordered sampling

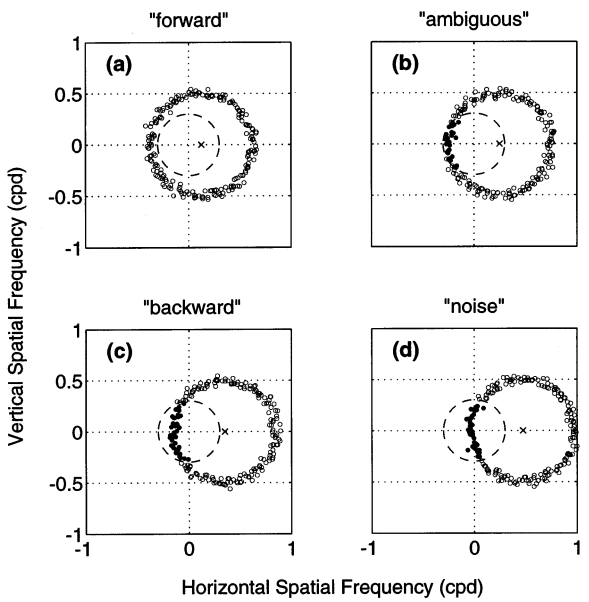

Fig. 1. Top down views (along the temporal frequency axis) of the spatio-temporal Fourier spectrum of a grating sampled by an irregular array (i.e. horizontal sections through the spectrum at a height corresponding to the drift frequency of the grating). (a) The Yellott ring (circles) is outside the window of visibility (dashed circle) and so only the leftward moving grating (x) is seen (note that input gratings are strictly speaking not visible, the delta functions (x) at the centre of the rings are shifted copies of the 0 cpd component of the sampling array spectrum which lodge themselves at the position of the input grating's frequency). (b) Both the grating and the alias (filled circles) are seen. (c) Only the backward moving alias, with an average orientation like the grating stimulus, is seen. (d) A stationary scintillating noise pattern is seen.

array, with mean detector distance $s \pm$ S.D., is a ring of noise with mean diameter $1/s$ [64,65] and a central delta function corresponding to the mean value of the sampling array (i.e. the [0,0] cpd component). The spectrum of a sampled image, is the convolution of the 'Yellott Ring' with the spectrum of the image. The action of sampling a grating pattern with a disordered sampling array is thus to create shifted copies of Yellott Rings centred on the delta functions representing the grating. As described by [52] it is the subsequent imposition of a post-sampling filter creating a window of visibility which results in the motion reversed percept. In the case of a human observer, this post sampling filter might occur in the visual cortex.

Fig. 1 shows a top-down view of some 3-D spatio-temporal spectra of moving gratings sampled by an irregular array (see [52]). If the grating spatial frequency is not too high the Yellott Ring is outside the region of visibility and not seen at all (Fig. 1(a)). At higher frequencies the Yellott Ring is seen exclusively and the predicted percept is that of a noisy grating moving backwards (Fig. 1(c)) with the same mean orientation as the sampled grating (cf. [66]), a lower mean spatial frequency and a higher velocity (the temporal frequency being fixed). At other spatial frequencies both the real and the aliased patterns may be seen simultaneously (Fig. 1(b)) or a stationary scintillating oriented noise pattern may be seen (Fig. 1(d), cf. [67]). In the case of two stage sampling of an image, first by the cones and then by ganglion cells, the situation is more complex but the first motion reversal seen as spatial frequency is increased still provides an accurate measure of the ganglion cell densities [53].

The above material leaves us with several expectations. If the FD illusion is produced by the M_y-cells then, just as s-cone (blue-cone) stimuli have been used to unmask aliasing effects in the human s-cone pathway (cf. [65] with [68,58]), FD stimuli could unmask the effects of undersampling in the M_y-cell array. In addition to observing motion reversal of moving FD patterns, the aliased patterns would have the appearance of a noisy grating, at times moving at a higher velocity than the input stimulus [52]. The value of S_c should be independent of parameters such as luminance, contrast, drift rate and viewing distance. Most importantly the values of S_c measured at different retinal eccentricities should indicate cell densities considerably below that of all M-cells.

2. Methods

In most experiments subjects had to indicate the dominant direction of translating sinusoidal gratings whose contrast was also modulated. Drift rates were in the range 1–4 Hz and flicker rates were in the range 20–30 Hz. Typically, nine spatial frequencies were used for a given experiment and gratings where presented within circular apertures. A tone (220 Hz) accompanied the onset of the gratings. Subjects signalled the perceived direction of drift by pressing a lever. Gratings where presented for 2 s and the subject also had the option of having the same grating presented again, but the direction of drift was randomised (left *vs* right, or up *vs* down, in a given experiment) for all presentations. Typically 15–30 repetitions for each grating were completed.

Two visual stimulus systems provided a control against hardware effects. Most experiments were conducted using a Barco CCID 7551 colour monitor (6500°K white), 45 cd m^{-2}, 480×512 pixels, 101 frames s^{-1}, usual contrast 0.9: visual stimuli generated by a Truevision Vista Board. A few experiments employed a white (P4 phosphor) Joyce monitor, 297 cd m^{-2} with 1024 scan lines at 200 frames s^{-2}, usual contrast 0.6, visual stimuli by a Joyce GR-SYS2. Non-linear systems analysis of c.r.t output confirmed c.r.t. linearity (e.g. [40]). We also examined S_c as a function of eccentricity, $S_c(x)$. The aperture diameters used at 0, 3.5, 10, 20, 30, 40° eccentricity were: 1, 2, 6, 12, 20, 25°, respectively. These apertures were selected as being the minium sized aperture providing reliable performance.

Correct judgements of drift direction were scored as a one and incorrect answers as a zero resulting in psychometric functions like those shown in Fig. 2(b), where a probability of zero indicates that a subject consistently sees the incorrect direction. The point of chance performance (i.e. $P = 0.5$) is referred to as a motion null, and to a first approximation the spatial frequency resulting in chance performance, i.e. $P = 0.5$, corresponds well to S_c [53]. The resultant psychometric function has the form of $1 - \mathit{erf}$ (erf = the error function i.e. the integral of a Gaussian), which is a function of (1) S_c and, (2) σ which is the slope at S_c. We fit the raw zero and one data to permit estimation of the error in S_c. Fitted values were obtained by a two stage process consisting of a graphical method followed by an iterative method.

The graphical method involved computing the cost, i.e. the mean squared residual, of fitting a small range of values of S_c and σ (typically 6400 pairs). This brute force approach had the advantage that one could graphically examine the 2-D cost (mean square residual) function to guard against selecting local minima. Usually a second and more fine grained inspection of the region around the initial minimum of the cost function was made and the results of this search were used as initial estimates for the iterative fitting method to find the absolute minimum. The iterative method was a Gauss-Newton technique. The shape of the cost surfaces, the estimated covariance matrix and subsequent Monte Carlo simulations showed that, S_c and σ

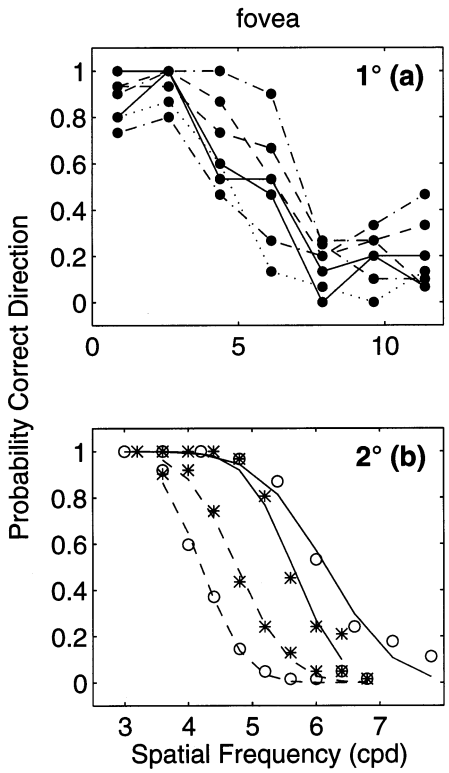

Fig. 2. Motion reversal for foveally presented gratings. (a) Psychometric functions for seven persons for the central 1° of the visual field. The gratings drifted at 2 Hz had their contrast modulated sinusoidally at 25 Hz, contrast 90%, N = 15, mean luminance 45 cd m^{-2}. (b) Examples of fitted (Methods) psychometric functions for two subjects (tm = solid curves; ghh = dashed curves) illustrating the range of the data for the central 2°. The gratings drifted at 1 Hz had their contrast modulated sinusoidally at 20 Hz, contrast 30%, N = 30, mean luminance 297 cd m^{-2}. Data were obtained at viewing distances of 81 cm (*) and 325cm (o). The spatial frequencies on the abscissa are twice the input spatial frequency, i.e. that of the illusory FD pattern (see Methods).

did not covary significantly and so univariate confidence limits were reasonable, and that the estimated errors were in accord with those obtained by simulation. A similar procedure was used to fit the functions describing the variation of S_c with retinal eccentricity, Eq. (1) below.

Well analysed data from macaques on the density of Magnocellular LGN cells as a function of retinal eccentricity are available [69] for comparison with the data and analysis to be presented. Data on the diameter of human parasol cells as a function of eccentricity is also available [28] but without knowing the coverage factors (estimates in macaque range from two to seven: [54,32,55]) these data are not accurately convertible to cell densities. Moreover, we do not know if the physiologically identified M_y-cells correspond to parasol cells. Van Essen, Newsome and Maunsell [70] introduced an empirically derived function to describe cell density as a function of retinal eccentricity of the form:

$$D(x) = k(a + x)^{-z} \quad (1)$$

where x is retinal eccentricity. Larger values of a produce flatter foveal densities while the asymptotic slope at high eccentricities is governed by z. Thus, $1/a$ governs the foveal retinal magnification and z the extrafoveal magnification. Connolly and Van Essen [69] employed further constrained the fitting of a by requiring that total number of cells within the central 2.5° of the retina, $N_{2.5}$, was correctly predicted by the fit. This was achieved by keeping the half volume of revolution (for a hemifield, i.e. one side of the dLGN) of Eq. (1) equal to the value of $N_{2.5}$. The same procedure was used here but $N_{2.5}$ was sometimes allowed to range over the confidence limits reported by Connolly and Van Essen [69] $\pm$ 50%. The values of $S_c(x)$ can be obtained directly from the density of cells as a function of eccentricity, $D(x)$, by:

$$S_c(x) = (D(x)/2\sqrt{3})^{1/2} \quad (2)$$

Notice that the values of $S_c(x)$ obtained from Eq. (2) assume a hexagonal packing of M_y-cells which is the best approximation for a disordered array [67].

Using the FD illusion as a probe of the density of the underlying sampling array can lead to conceptual problems because the stimulus is the spatial second harmonic of the input spatial frequency. We mention here some of these problems, and our rational for presenting the results as we do, so that Section 3 can be interpreted more easily. We report our results in terms of the FD spatial frequency unless otherwise mentioned. Use of FD stimuli raises another problem in terms of ON- and OFF-cells. If the FD illusion arises as the result of full-wave rectification [2,7] in Y-like cells, and given that the rectified responses arise from a different source than the linear response (the quadratic response arising from separate nonlinear subunits [15,16,6]), then rectified responses in the ON- and OFF-centred Y-cells will have the same sign. This admits the possibility of the ON- and OFF-units acting as a single array with twice the density. Since we are often using motion detection in our experiments, and given that the most likely form of motion computation requires separate ON and OFF channels [71,72], we may be measuring the density of these paths separately. A final possibility is that the full wave rectification renders the nonlinear information in ON- and OFF-channels the same and so unfit for motion computation, and instead the direction of motion may be based on the linear response components of the M_y-cells. In this case the spatial frequency of the percept is determined by rectification but the perceived motion is determined by the linear response component. The initial fits to Eq. (1) are done assuming a single array and the question of separate ON and OFF arrays, and linear *versus* nonlinear responses is addressed in Section 4.

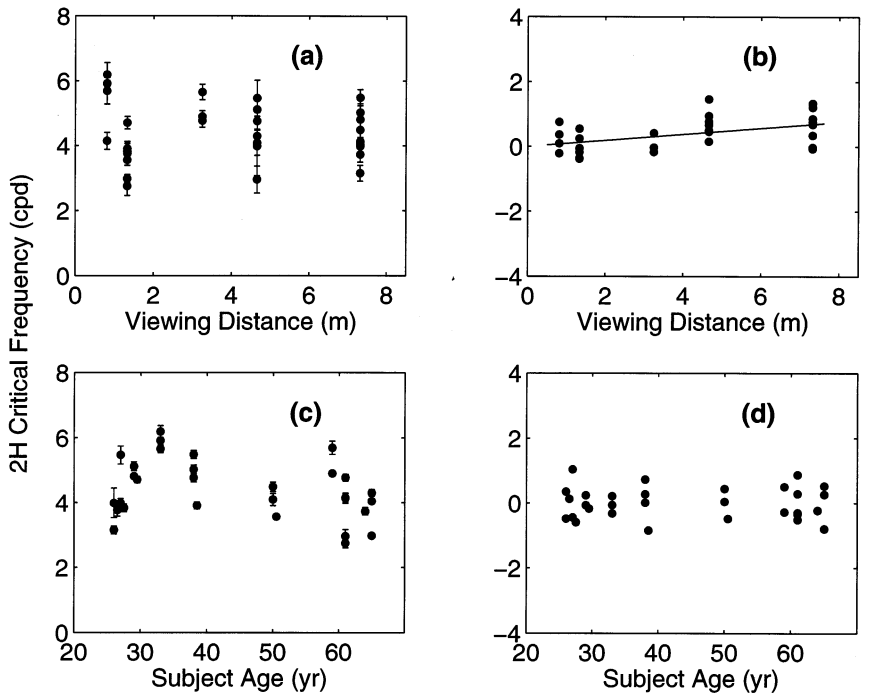

Fig. 3. Dependence of the critical spatial frequency S_c upon viewing distance and age for eight subjects for the central 2° of the visual field. (a) Raw viewing distance data. (c) Raw data for age. Strong subject effects and a weak effect associated with some data taken at a higher luminance and a different test situation (Methods) were characterised by a multiple regression. (b) Residuals plotted against viewing distance after effects of subject and test site are removed. The slope of the (solid) regression line (0.094 ± 0.043se cyc $^{\circ -1}$ m^{-1}) is significant ($P = 0.04$) but is it is 11 times smaller (21 standard errors) than if the number of cycles on the c.r.t. determined S_c. (d) Residuals after fitting viewing distance also showing no significant age dependence of S_c.

3. Results

Motion reversal was observed for drifting FD test patterns. Subjects often reported that near S_c two patterns were simultaneously visible as transparent sheets: the drifting FD pattern and a wiggly grating moving in the opposite direction to the FD grating (cf. Fig. 1(b)). The spatially wiggly, or broken up, appearance of the reversed percept is consistent with the aliased pattern being spatially and orientation band limited noise [52]. Also, as predicted for an alias, the motion reversed pattern often moved at a higher angular velocity than the input. At spatial frequencies further above S_c the reversed percept became dominant (cf. Fig. 1(c)). When two patterns were evident subjects reported which was most vivid.

The central visual fields of seven subjects were tested with gratings presented within 1° apertures (Fig. 2(a)), and eight subjects were tested with 2° apertures (Fig. 2(b) and Fig. 3). The mean values of S_c obtained for the 1 and 2° apertures were 6.12 ± 0.37S.E. and 4.86 ± 0.19S.E. cpd, respectively. Subjects showed noisier performance with the smaller aperture reflecting the greater difficulty of the task. Note that these values refer to the FD illusory spatial frequency. The most obvious feature of data is that the subjects clearly experienced a reversal of the perceived grating motion, i.e. their ability to guess the correct direction went to near zero probability as spatial frequency increased.

Multiple measurements from eight subjects where S_c. is examined over a 9 fold increase in viewing distance and where subject age varied over four decades is summarised in Fig. 3. The raw data for the effect of viewing distance and age are presented in Fig. 3(a,c). The data were submitted to a multivariate regression against several factors. There was a significant subject effect ($P = 0.02$), i.e. different subjects had different S_c. This had been indicated by the relatively small standard errors in comparison to the scatter of the points in Fig. 3(a,c) (and see Fig. 2(b)). Also, fitted was a factor associated with the two experimental setups (see Methods) with which data were collected. Seven of the 30 points, from three of the eight subjects, were collected at the higher luminance of 297 cd m^{-2}, the remainder being measured at 45 cd m^{-2}. This factor was significant ($P = 0.005$) and acted to increase S_c by 1.2 ± 0.30S.E. cpd at all viewing distances.

The residuals obtained after removing the effects of subject and test conditions show the independent effects of viewing distance (Fig. 3(b)) and age (Fig. 3(d)). There is a slight trend towards a higher S_c with increasing viewing distance (slope $= 0.094 \pm 0.043$S.E. cycles $^{\circ -1}$ m^{-1}, $P = 0.040$). The slope is significantly different ($t = 21.0$, d$f = 20$) to that expected if the reversal effect

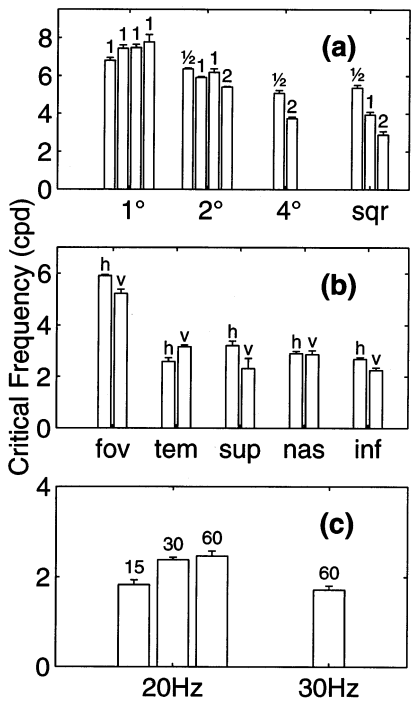

Fig. 4. S_c changes as a function of the area of retina stimulated but not other image parameters. (a) The effects on the measured S_c of presenting the gratings within circular apertures of 1, 2 and 4° diameter and a 3.6° square aperture (sqr). Lower values of S_c are measured as more of the peripheral retina is recruited. The small numerals above the bars indicate the drift temporal frequencies used. (b) S_c measured in the central 2° (fov), and for 2° apertures presented at 3.5° eccentricity in the temporal (tem), superior (sup), nasal (nas) and inferior (inf) visual fields. The small **h** or **v** atop each bar indicates the grating orientation. (c) S_c determined for several octaves of contrast (left 3 bars, numerals indicate % contrast) using sinusoidal contrast modulation of 20 and 30 Hz, drift 2 Hz, aperture 4°. For (a) to (c) Mean luminance 297 cd m^{-2}, frame rate 200 Hz.

depended upon the number of cycles on the c.r.t (i.e. slope = 1). Clearly the motion reversal depends upon spatial frequency rather than upon grating size. There was no significant trend with subject age (Fig. 3(d)). Age data was somewhat correlated with subject but most subjects were tested in two sessions six months apart and three subjects were also tested five years apart permitting some independent estimation of age and subject effects.

Decreasing values of S_c are expected for increasing aperture sizes, given that retinal cell densities fall-off with eccentricity. Fig. 4(a) shows S_c values obtained from central retina (subject tm) where increasing aperture diameters of 1, 2 and 4° produced a consistent downward trend in S_c, as less dense parts of the retina are recruited. Fig. 4(b) illustrates results from experiments where gratings were presented in 2° apertures centrally and at 3.5° eccentricity in the superior, inferior, temporal and nasal visual fields. Again the data indicate that S_c is linked to retinal magnification. S_c values did not otherwise change for over several octaves of drift frequency (Fig. 4(a)), or grating contrast (Fig. 4(c)). Aperture shape (Fig. 4(a)) and grating orientation (Fig. 4(b)) also did not change S_c.

Fig. 5(a) shows results where a broader range of spatial frequencies was examined looking for a second motion reversal irrespective of the spatial appearance of the stimuli. We did not observe a second motion reversal (Fig. 5(a)) (as predicted by Galvin *et al.* [53]). Instead as spatial frequency increases subject performance asymptotes to chance performance (0.5) where the stimuli soon become too demodulated to see. It is likely, however, that FD illusion itself may break down at spatial frequencies around $2S_c$ (Fig. 5(b)) as is expected from Y-cell physiology [38,5] and previous experiments on the illusion [1]. To investigate this possibility subjects compared the spatial frequency of gratings, contrast modulated at 25 Hz, subsequently presented, temporally unmodulated, versions of the same gratings. Subjects had to report whether the perceived spatial frequency of the grating was finer or equal to the unmodulated version of the same grating. This procedure illustrated that by about $2S_c$ (14 cpd) spatial frequency doubling was no longer observed (Fig. 5(b)).

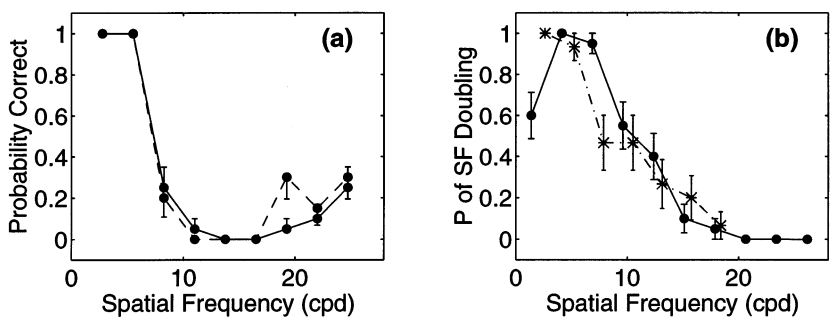

Fig. 5. Motion reversal and the FD illusion at higher spatial frequencies. (a) Two repeats where the task was to determine the direction of the dominant motion. Both targets were presented to the central 1° of the right eye of tm. There is no second motion null near 14 cpd. (b) Two subjects (* = kr, ● = tm) compared the apparent spatial frequency of gratings modulated at 25 Hz with the same grating with no temporal contrast modulation.

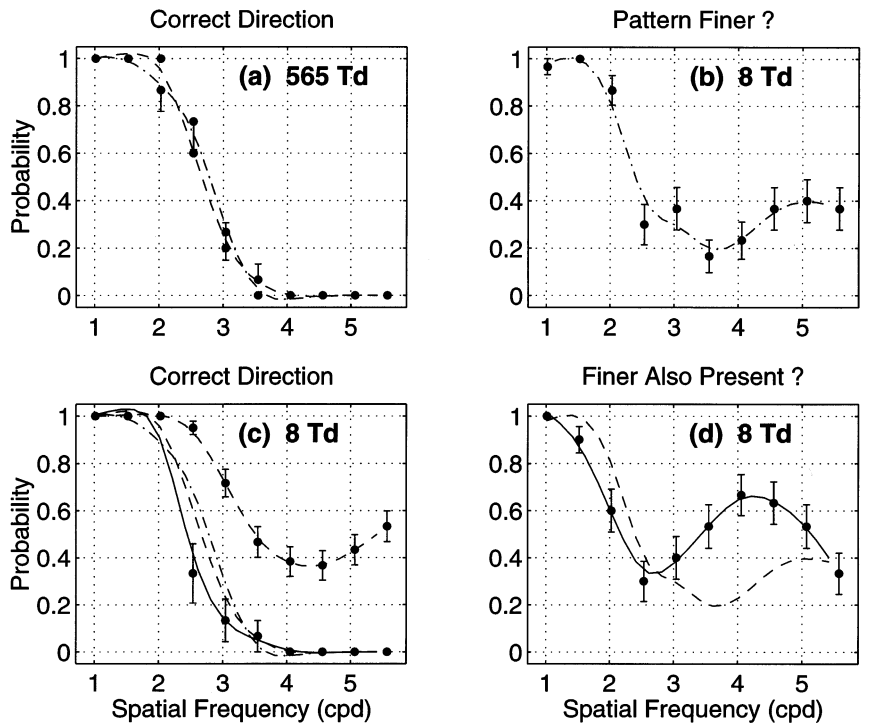

Fig. 6. (a) Motion reversal characterised for 16.7 (dashed, N = 30) and 25.1 Hz (dash dot, N = 30) flicker at 565 Td. (b) The dashed curve shows (at 8 Td) the probability of the 16.7 Hz flickering grating having an apparently higher spatial frequency than the same grating unmodulated. (c) Motion reversal at 8 Td and 16.7 Hz (solid, N = 45) compared with (a) (dot-dashed) and Motion reversal at 8 Td 25 Hz (dashed). At 25 Hz and 8 Td although the gratings are evident picking the direction of movement is difficult reducing the ability to see reversals (N = 60). (d) The solid curve indicates the probability of a finer pattern also being apparent. The second peak near 4 cpd suggests that at this low luminance a trace of the predicted alias is visible against a stronger linear response. The dashed curves are from (b). Retinal illumination = 8 Td, N = 45 for all curves. Curves in (a) to (d) are cubic splines (with constrained bending energy) and are shown to aid visualisation. All data obtained for the central 4°. Error bars are S.E., in (a) the upper or lower error bars are shown on each curve.

Some experiments were conducted at low retinal illuminations to examine what happens as cone input degrades. Fig. 6(a) shows psychometric functions characterising motion reversal at 565 Td (45 cd m^{-2}, 3 mm pupil) obtained at 25 and 16.7 Hz contrast reversal rates. These two curves are reproduced in Fig. 6(c) [dash-dot lines] for comparison with another two psychometric functions obtained at 16.7 and 25 Hz and 8 Td (1.13 cd m^{-2}, 4 mm pupil: solid and dashed lines). We used 16.7 Hz flicker at 8 Td when we found that we could not measure a strict motion reversal at 25 Hz (Fig. 6(c), dashed) because the gratings appeared too faint leading to near chance performance above 3 cpd. The observed demodulation is in agreement with M_y-cell physiology [34], where it has been shown that below 20 Td individual cell responses to higher frequencies begin to decline. Data presented in Fig. 6 were obtained with an aperture diameter of 4°: larger apertures were required to obtain reasonable accuracy at the lower luminances.

An interesting fact emerged in experiments examining the apparent spatial frequency of gratings at 8 Td. The dashed curve of Fig. 6(b) shows the outcome if the question is asked: 'is the apparent spatial frequency of the 16.7 Hz modulated grating greater than its unmodulated self?'. The results are quite similar to Fig. 5(b) except that there is a greater tendency toward 50% performance at higher frequencies. In the course of these experiments it became clear that not infrequently two image components were simultaneously visible, one coarser pattern, similar to the input test pattern; and one noisier finer spatial frequency component (the expectation above $2S_c$). The solid curve of Fig. 6(d) is the psychometric function obtained when the question is asked 'is an image component finer that the unmodulated reference pattern also present?' Under this condition the finer component is visible in two spatial frequency bands with a second peak around 4 cpd.

3.1. Dependence of S_c upon retinal eccentricity

Measurements of S_c as a function of eccentricity, $S_c(x)$, were obtained for the temporal visual field of seven subjects and from the nasal visual field of four of those subjects. These measurements where made on the Barco based system (45 cd m^{-2}, 25 Hz flicker) on all seven subjects including tm, and on the Joyce system (297 cd m^{-2}, 30 Hz) only for tm. The basic paradigm

Table 1
Fitted parameters for Eq. (1) for the nasal and temporal visual fields of six subjects, showing mean values for the temporal, nasal and both visual fields

Test	a (deg)	z	k (cells/deg^{-2})	$N_{2.5}$ (cells)	Subject
Temporal	1.48	1.77	399	2300	tm[a]
Visual	1.09	1.57	210	1800	tm
Fields	1.55	1.96	357	1600	acj
	0.97	1.79	109	900	mri
Nasal	0.91	1.54	177	1800	tm[a]
Visual	0.83	1.37	141	1800	tm
Fields	0.78	1.67	123	1300	pjs
	3.04	1.59	606	2100	mih
Means					
Temporal	1.27	1.77	269	1650	
Nasal	1.39	1.54	262	1750	
Both	1.33 ± 0.26	1.66 ± 0.06	265 ± 62	1700 ± 156	
Temporal [69]	3.94	1.54	495	1400	
Nasal [69]	2.25	1.44	293	1700	

The last two rows are based on anatomical data from Connolly and Van Essen [69]. The right-most column denotes the subject, errors are S.E.
[a] Measurements at a mean luminance of 297 cd m^{-2}, all others at 45 cd m^{-2}.

was to measure S_c at variety of retinal eccentricities and then to fit the resultant values to Eq. (1) after first converting the S_c values to cell density by use of Eq. (2). The densities where then scaled by a density fraction ρ_y which was an estimate of the proportion of dLGN projecting M-cells which are M_y-cells, on the assumption that the M_y-cell density would be a simple scaling of the M_x-cell population as is found for cat X and Y-cells [73].

Eight data sets, four from nasal retina and four from temporal retina showed a global minimum when fit to Eq. (1) (Table 1). The other three data sets did not converge to a unique solution (but see below). Fitted $S_c(x)$ curves obtained for the four temporal visual fields are shown in Fig. 7. Fig. 8(a) shows the progress of the fitting process by showing the trajectory, parameterised in $N_{2.5}$, of the global minimum computed for each set of a, z (k being determined by $N_{2.5}$) illustrating that the overall minimum cost (mean square error) was obtained near $N_{2.5} = 1800$.

Of most interest are the values of z and $N_{2.5}$ because these parameters ultimately determine the intra- and extra-foveal magnification, also there is a natural tendency for k to rise to compensate for rising a (i.e. a and k covary). Values obtained here for a, the foveal magnification, are more likely to be correct than fitted values derived by Connolly and Van Essen [69] given that here density data inside the central 2.5° was available, rather than $N_{2.5}$ alone. The values of z and $N_{2.5}$ (Table 1) are in good agreement with Connolly and Van Essen [69]. To aid comparison with Connolly and Van Essen [69] the values of k and $N_{2.5}$ shown in Table 1 were scaled by the fraction of M-cells which are Y-like, ρ_y, to describe the total M-cell population.

In the actual fits to the data derived from S_c measurements the values used were based on $\rho_y * k$ and $\rho_y * N_{2.5}$ to provide the M_y-cell densities for a given S_c. For all estimated parameters in Table 1 ρ_y was set to 0.25 implying that the Y-like cells are about 0.25 as dense as parasol cells. A ρ_y of 0.25 was about as low as could be obtained with a $N_{2.5}$ like that of Connolly and Van Essen [69]. It is important to understand the exact figure is entirely dependent on the value of $N_{2.5}$ for humans, which is unknown. If $N_{2.5}$ is larger for a human then the value of ρ_v drops. Changing $N_{2.5}$ only changes k not a or z.

Our fitted values of k are smaller than those of Connolly and Van Essen [69] by 0.60 (1062/1760). Similarly, the maximum value allowed by Connolly and Van Essens [69] estimates of error for their value of $N_{2.5}$ is 2550 which is 1/0.67 greater than the mean value shown here of 1700. Thus, with no effect on the goodness of fit, and operating within the limits described by Connolly and Van Essen [69], we can assume a value of $N_{2.5}$ of 2550 and so our becomes: $\rho_y = 0.6 * 0.25 = 0.15$. Our k values then also agree with the macaque data.

At alternate method was tried in order to use all our data to obtain a better estimate of ρ_y. This approach recognised the fact that z is likely to be a fairly well conserved parameter. We therefore fixed z at our mean value of 1.657 (± 0.1539, 95% confidence limit for $df = 7$) and refit our 11 data sets. Note that varying $N_{2.5}$ in the fitting process is the same as fitting ρ_y assuming $N_{2.5}$ fixed. By fixing z, and thus reducing the number of fitted parameters, all our 11 data sets produced a global minimum, an example being shown in Fig. 8(b). The trajectory plotting the course of fitting is now parameterised in ρ_y and the numbers shown assume $N_{2.5} =$ 1800. If a value of $N_{2.5}$ of 2550 is assumed the

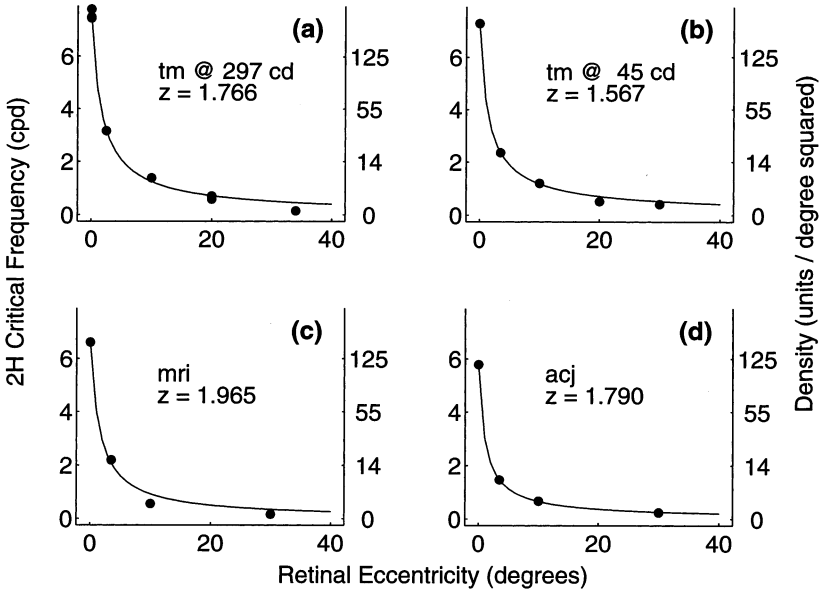

Fig. 7. The dependence of S_c upon nasal retinal eccentricity, $S_c(x)$, for the temporal visual field of four subjects. The solid curves represent fits to $S_c(x)$ assuming 25% of M-cells are M_y-cells (i.e. $\rho_y = 0.25$). This represents an upper bound on ρ_y, the lowest estimate being 5.4% (see text). Right ordinate = cell densities, $D(x)$ (Eq. (1)). The mean luminance at which the measurements were made is shown in the inset along with the subject label. The fitted exponent z is also shown in each panel.

minimum in Fig. 8(b) would be at $\rho_y = 0.13$. The mean value of ρ_y for the 11 data sets was 0.151 ± 0.035 S.D., in agreement with our estimate of 0.15 in the previous paragraph. Also noteworthy is the fact that, even assuming $N_{2.5} = 1800$, values of ρ_y much larger than 0.25 are decidedly unfavoured as shown by the rapid rise in mean square error (Fig. 8(b)). Clearly the sampling mosaic used in seeing the spatial frequency doubled illusion has a density less than 20% of the total M-cell population.

At-test of the hypothesis that z (Eq. (1)) is larger than that for the nasal field for data from seven subjects was significant ($P = 0.03$). $S_c(x)$ from inferior and superior visual fields were also obtained for one subject (tm) and these data required $z > 2$.

4. Discussion

4.1. Evidence for aliasing

Data from eight subjects indicate that the observed motion reversal effect is determined by spatial frequency rather than viewing distance or age (Fig. 3). Several octaves of contrast, drift frequency, and mean luminance have little or no significant effect on S_c (Fig. 4 and Fig. 6(c)). The slight (much less than two octaves) trend towards lower S_c with two octaves of drift rate (Fig. 4(a)) may be due to the temporal qualities of the post-sampling filter [52]. Similarly, grating orientation and contrast modulation frequencies over the range 20—30 Hz (Fig. 3 and Fig. 4(c)) also have little effect upon S_c. The tests employing different grating orientations showed that the alias was always motion reversed indicating the sampling array is disordered in all orientations [52,63]. An effect associated with test apparatus, or a 6.6 times change in luminance, significantly shifted S_c for the central 2° upward by 1.2 ± 0.3S.E. cpd (25%). Several factors such as subject experience, years between measurements and a darker background field, are confounded with this factor so it is difficult to judge its meaning. Subsequent examination of S_c at scotopic luminances (a 68 fold reduction) indicates very small luminance effects (Fig. 6(c)). So on balance it is clear that spatial frequency is the major determinant of the motion reversal effect, as required for spatial aliasing. It is also worth noting that the experiments at 8 Td eliminate a nonlinear interaction between L and M cones in the surrounds of M_x-cell receptive fields [74] as the source of the FD illusion.

Also as predicted (e.g. Fig. 1(b)) at frequencies near S_c subjects report seeing both the aliased percept and the grating stimulus. This motion transparency effect indicates that the underlying process by which direction of the drifting FD gratings is detected is a non-opponent system [75] as embodied in directionally selective complex cells [71,72]. More generally the motion reversed pattern has the appearance of spatially low pass noise with the mean orientation of the stimulus grating, i.e. a slightly wobbly or fractured grating, but often moving at higher velocities. These higher velocities are also a predicted feature of a spatial alias (Fig. 1(b)).

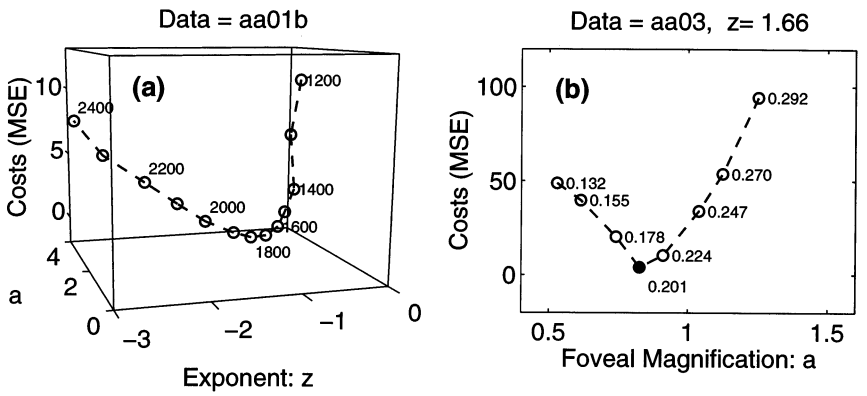

Fig. 8. Trajectories of fitting process for an $S_c(x)$ data set. (a) The mean square error (MSE) for different fits of the parameters a, z, from Eq. (1) and $N_{2.5}$. The trajectory is parameterized in $N_{2.5}$ and each point (o) represents the global minimum. There is a global minimum near $N_{2.5} = 1800$. (b) The same data set is force fit with the mean value of $z = 1.66$. Now the trajectory showing the MSE for each value of a is parameterized in ρ_y, the proportion of Y-like cells. A clear minimum occurs near $\rho_y = 0.20$.

It is important to recall that it is unlikely that all trace of other ganglion cell types is extinguished when the FD illusion is observed. For example, at photopic luminances P-cells can respond to quite rapid contrast variations, albeit weakly [16,30,34]. At lower luminances M-cell responses are stronger probably due to their strong rod input [76], while perhaps 20% of P-cells receive strong rod input [77] this input only seems to contribute minimally to P-cell responses and only below 2 Td [78]. M_y-cells also are the most Weberian of ganglion cells, maintaining their response to contrast and dynamic character to very low light levels, better even than M_x-cells [34]. At 8 Td, 16.7 Hz is still above the flicker fusion rate for P-cells [34]. Thus, at low luminances we might expect the masking effects of input from other ganglion cell types to be smaller and M_y-cell responses to be relatively larger. Scotopic conditions may also reduce the system to a single stage sampling process because the electrical coupling between rods, and between horizontal cells, would virtually eliminate aliasing at the rod and rod bipolar levels. This would predict a weak alias signal around $2S_c$ as observed at 8 Td (Fig. 6(d)). Taken together all the above observations strongly indicate that the motion reversed pattern is an alias.

Some further consideration of the contrasts we used and the circular apertures employed should be made because the hard edges could introduce orientation information making direction discrimination more difficult. At first glance the contrasts used seem high: 0.9 for most of the Barco experiments and 0.6 for most Joyce experiments; however, due to the high modulation rates (typically 25 and 30 Hz, respectively) the subjective contrast was less than half the actual input contrast. Also, experiments using 15, 30 and 60% contrast yielded very similar results for S_c (Fig. 4(c)). Experiments at low luminance, particularly at high flicker rates (Fig. 6(c)), produced very low subjective contrasts and yet the measured S_c was little different than at high light levels. Thus, several experiments indicate that contrast had little effect on S_c, and so any edge effects at the higher contrast conditions appear to have been minimal.

Our fits to $S_c(x)$ assumed that both the ON- and OFF-centred My-cells are contributing to the same array. As mentioned in the Methods this is not unreasonable given the way in which the nonlinear response is generated. In both primate [15,16] and cat [38,5] there is good evidence that the nonlinear response arises from a separate source, an array of full wave rectified subunits, and that this is added on to the Y-cell response [6]. This means that the second harmonic responses in both ON- and OFF-centred units will have the same sign and so the two groups of cells could be acting as a single array. We do, however, exploit neural motion detection in our experiments and the most likely form of motion computation requires separate ON and OFF channels [71,72], therefore we may be measuring the density of these paths separately. In that case ρ_y would be 0.302 ± 0.022S.E. ($N = 11$). The aforementioned possibility that the motion reversal is based on the linear response component of M_y-cells will be addressed once the effects of sampling by multiple arrays is discussed.

Connolly and Van Essen [69] found that z (Eq. (1)) was larger for LGN laminae corresponding to the temporal visual field in both the Magno- and Parvicellular layers which is in line with differences in ganglion cell densities seen in the macaque [54,79,80] and human [27,28]. Similar results for $S_c(x)$ where also found here. Results from inferior and superior visual fields required $z > 2$, similar exponents were obtained by Schein [81] when fitting the cone densities of the macaque superior and inferior retina.

4.2. Alternatives for the motion reversal

A possible concern is that the reversed motion percept may actually be part of the stimulus and not a spatial alias at all. This arises from the fact that a grating moving to the left drifting left at 2 Hz (f_d) and modulated at 25 Hz (f_f) can be thought of as the sum of a grating moving left at 27 Hz (f_d+f_f) and a second moving right at -23 Hz (f_d-f_f). This permits the possibility that below a certain spatial frequency (near S_c) the FD illusion is strong and the FD grating is seen to move in the correct direction, while above that spatial frequency, the FD illusion is not seen or is seen poorly, and for some reason the -23 Hz grating alone is seen instead. Control experiments on five subjects (not shown) indicated that the drift velocities observed where that of an alias and not that of the much faster f_d-f_f component.

The motion reversal effect reported here also does not appear to be related to the motion reversal effected investigated by Chubb and Sperling [82]. There are several reasons why these phenomena are unlikely to be related. The stimuli used by Chubb and Sperling were narrow stripes which were jumped by a quarter wavelength and then contrast reversed. Above a certain spatial frequency the stripe patterns appear to move in the reversed direction. It appears, however, that the effect breaks down totally at temporal frequencies above 10 Hz [83,84]. Also the reversed motion percept produced in these cases does not move at a higher speed than the stimulus, and does not have the noisy appearance of an alias. Therefore the phenomena reported by those authors do not appear to be related to motion reversal of FD patterns.

Another effect which could theoretically produce low S_c values even for a denser set of cells, say the array of all the M-cells, is so called multi-rate sampling [51]. The effect occurs in highly orderly multilayer sampling arrays where there is divergence and convergence of information not unlike the retina. Several factors discount this possibility. The first of these is that all such systems also appear to provide a vivid alias for input at 0 cpd (a process called imaging) which is not observed. More importantly it is unlikely that the sampling matrix of M_y-cells is highly regular given that the alias has the same orientation as the input grating (cf. [63,52]).

4.3. The linear response

The finding that a second motion reversal was not observed at $2S_c$ meets the expectation for a two stage sampling process, where both cone and ganglion cell array effects need to be considered [53]. Several other factors could contribute to a lack a second reversal and we discuss them below.

This study was partially predicated upon the observation that the highest spatial frequency the individual M_y-cells respond to, at any particular eccentricity, appears to be about four to eight times higher [17] than the M_y-cell Nyquist frequency predicted from anatomical data [69]. Naturally, the linear response component will also alias once the Nyquist rate is exceeded: the FD stimuli used here only being necessary to unmask M_y-cell responses from the responses of other cells. Therefore, as spatial frequency is increased, and the FD frequency exceeds $1.5S_c$, one would also begin to see an aliased component arising from the fundamental (linear) response component. This would have the effect of stretching the band of frequencies over which motion reversal is reported as in Fig. 5(a). So, while there is evidence of an alias pattern with the correct spatial appearance in the band $1.5–2S_c$, the FD component is likely to be weak (Fig. 5(b)) and perhaps masked by contributions from other cell types, especially at higher luminances, as well as by the linear response component of the M_y-cells themselves.

The point has been raised that full wave rectification would lead to identical signals in the ON- and OFF-sub M_y-cells at a given retinal position. This might affect our ability to observe any image motion. This opens up the possibility that while our visual percept is the FD illusion, the motion computation is actually based on smaller linear response components of the M_y-cells. In this case we should have used the input spatial frequencies to calculate ρ_y. For this reason we ran the calculation again on the 11 $S_c(x)$ data sets, using the fundamental spatial frequencies as inputs and keeping the exponent z fixed at 1.657. The new mean value of ρ_y was 0.027 ± 0.004S.E., assuming an $N_{2.5}$ of 1800. Doubling this for separate ON- and OFF-streams yields a ρ_y of 0.054. This is towards the lower limit of the estimated fraction of M_y-cells (e.g. [30]).

The difficulty with the linear Y-cell response determining S_c is of course that it raises the question: why don't the linear M_x-cells determine the perceived direction of motion if processing the weaker linear response is an option? One answer could be that once the brain has decided that the second harmonic response from the Y-like cells is the correct percept that only information from that stream can be used to compute motion, thus excluding linear M_x-cell responses, and forcing M_y-cell linear input to be the signal used for motion computation. A similar argument may apply to recent observations that P-cells, rather than M_x-cells, determine the upper spatial limit for motion computation [62,59,53]. Thus, perhaps when P-cells provide the best percept (by some unknown criteria, perhaps signal to noise ratio at high spatial frequencies) they are exclusively used for motion computation and not M-cells. A mechanism which can select the most reliable input stream(s) for motion computation would also be com-

patible with some higher order motion processing schemes [85].

4.4. If M_x-cells display some Y-like activity would this affect the measured S_c?

X-cells can show some quadratic response especially at lower spatial frequencies [86] Fig. 5. For these cells to have no effect whatsoever upon the observed S_c it is only necessary is that the Y cells and the X cells have a different mean inter-cell distance, which we might refer to as d_y and d_x. There could be considerable noise in the inter-cell distance but, irrespective of the noise, as long as there was a mean difference between d_y and d_x then this defines two disordered sampling matrices having two different values of S_c, exactly equal to $1/2d_y$ and $1/2d_x$ [52].

Fig. 9 is provided to illustrate what happens in the case of combining a coarser and a finer sampling array, like possibly the X and Y-like Magnocellular units, with critical frequencies $1/2d_y$ and $1/2d_x$. Fig. 9 is like Fig. 1 but includes a larger outer Yellott ring, corresponding to the array with mean intercell distance d_x.

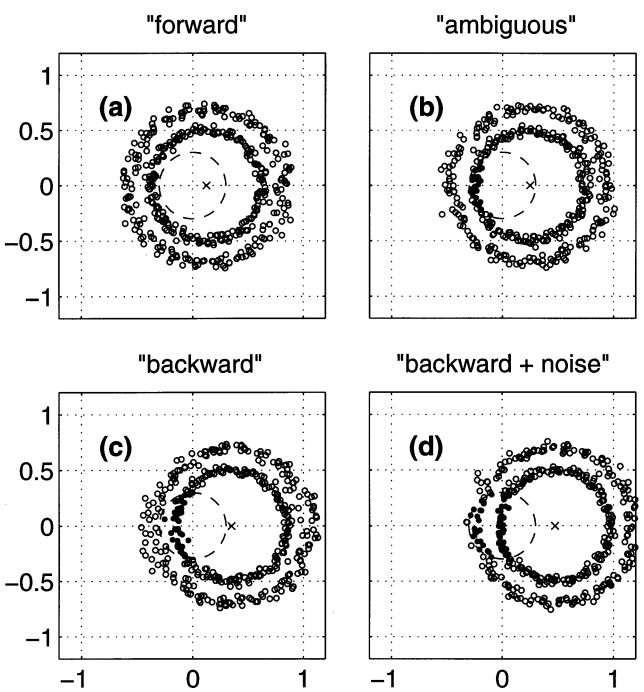

Fig. 9. The effects of a second array with a higher density of cells upon the first motion reversal (cf. Fig. 1). The (x) indicates the spatial frequency of the input pattern. (a) Neither Yellott ring can be seen as the window of visibility imposed by post sampling filtering is too constrained. (b) The first motion reversal is seen, there is no effect form the outer ring arising from the higher density units. The (x) indicates that the input pattern is seen simultaneously. (c) Motion reversal still apparent, input grating no longer seen. (d) At sufficiently high input frequency the outer ring from the denser array becomes visible broadening the range of frequencies over which motion reversal is seen.

Note that the onset of the first motion reversal will be completely unaffected by the second ring because the inner ring precedes the outer ring into the window of visibility (e.g. Fig. 9(c)). The effect of the second ring is only observed when the spatial frequency of the input grating (the x) is sufficiently high that the outer ring begins to intrude into the window of visibility (Fig. 9(d)). As shown in Fig. 9(d) this could have the effect of extending the range of spatial frequencies over which motion reversal is observed as in fact occurs (e.g. Fig. 5(a)).

One additional fact must be noted: even if the denser array had 95% of its sensing elements turned off at random the S_c of the denser array is unchanged! This behaviour of so called degenerate arrays was elegantly demonstrated by Geller *et al.* [87]. No knowledge of Fourier analysis is required to understand that the Nyquist rate for a degenerate sampling array is the same as the complete, parent, array. If some elements are removed at random from a disordered array there will always be elements with the original inter-element distance d, leading to a spectrum with a mean radius $1/d$. The corollary for the present argument is that: even if a random subset of X-cells were producing second harmonic responses, the diameter of the Yellott Ring for that subset of X-cells is the same as that of the whole X-cell array.

Therefore, as long as the M_y- and M_x-cells have a different mean inter-cell distance the effect of switching some X cells to partial or full Y-like behaviour will have no effect upon the diameter of the inner Yellott ring and therefore no effect upon the spatial frequency at which the first motion reversal is first seen. Even if some nonrandom (i.e. complex) system changed the mean inter-cell distance as some X cells became Y-like this would again not alter the diameter of the inner ring and so the first motion reversal would be unaffected.7

4.5. Is the nonlinear pathway the M_y system?

Perry *et al.* [29] found that about 10% of retinal ganglion cells project to the magnocellular layers of the dorsal LGN. Of these cells it appears that only 5–20% show the Y-cell response signature, i.e. the presence of a strong second harmonic response [15,16,30,17]. There is substantial evidence, both anatomical [26–28] and behavioural [23–25] that macaque retinas and their visual brain [88] are good models of the human system.

Several findings lend support to the correspondence between the nonlinear pathway described here and the M_y system. Firstly, cells of the magnocellular LGN of macaques are tuned to higher temporal frequencies than are cells in the parvicellular layers, the peak frequencies for the M and P cells were reported by Derrington and Lennie [30] as being 13.8 ± 6.1 Hz (P) and 21.5 ± 11.3 Hz (M), and by Marrocco *et al.* [16] as

10.9 ± 1.04 (P), 19.5 ± 6.8 (M_x) and 19.6 ± 5.0 (M_y). This difference between the P and M streams is in agreement the findings of Merigan and Eskin [89] on the contrast sensitivity of Macaques which have lost most of their P ganglion cells, through acrylamide monomer lesion. Merigan and Eskin [89] demonstrated that below 1 cpd and above 10 Hz contrast thresholds seem unaffected in these P-cell lesioned macaques. Thus, it appears that the M cell pathway dominates this region of spatio-temporal visual space [90,91], which corresponds to the domain where the frequency doubled effect is seen [1].

None of this, however, explains why the M_y subsystem might come to dominate the visual percept. Some evidence for Y-cell involvement comes from the fact that Y-cell quadratic responses (e.g. second harmonic responses) and the FD illusion both appear to be produced by a nonlinearity where the response is proportional to $|\text{contrast}|^z$, where contrast is signed and the exponent z is about 0.7 (cf. [5,6] and [7].

The retinal gain control effect described by Shapley and Victor [35] may explain the source of the FD illusion. The gain control operates such that at moderate to high temporal frequencies the response to increased contrasts is amplified. In the cat the retinal gain control is strongest in the Y system [38,5,39]. In the monkey all the properties which identify the Y response signature, such as the periphery effect [15] and spatial tuning of the quadratic response being indicative of subunit structure [15,16] have been found for primate M_y-cells. Retinal gain control has been confirmed in primate M-cells [30,36] and is not present in P cells [36]. For visual stimuli that would produce the FD illusion in humans this gain control is switched on and Y-cell second harmonic responses can be ten times the linear response [5,39]. Also P-cells are quite linear, eliminating them as sources of second harmonic responses. Recent PERG studies indicate that when conditions for seeing the FD illusion are approached, the PERG signal [40–42] becomes dominated by responses showing phase shifts indicative of the action of retinal gain control upon the second harmonic responses of Y-type cells [39].

Other effects such as the action of cortical efferents upon LGN neurons may also play a role in unmasking the FD illusion [92]. Selective suppression of particular input streams to the cortex are known from saccadic suppression effects [93]. Therefore the effects of retinal gain control in the production of the FD illusion may be assisted by other mechanisms which either enhance the M pathway or suppress other retinal afferent pathways. So we find that by a number of mechanisms, principally retinal gain control acting upon M_y-cell quadratics responses, we might expect the visual percept to be substantially influenced by M_y-cells.

4.6. Evidence for a separate array of Y-like M-cells

In most mammals investigated there appear to be discrete X and Y types and these are quite differentiable on the basis of cell size [94]. To say that primates would not have the same arrangement is to say that they must be markedly different from other mammals. As described by Kaplan *et al.*, [95] in their review of primate ganglion cells the suggested figure of 15–30% of M-cells being Y-like is in good agreement with the known numbers of Y-cells in '20 species of placental mammals from six orders'. Perhaps the more likely case is then that in primates the expected size difference between X and Y cells (in the Magnocellular pathway) is simply smaller making the usual anatomical discrimination difficult. Sterling *et al.* ([96], and Calkins personal communication) have made a case for the 'Garland' type retinal ganglion cells being the Y-like M-cells based upon their stratification, their connection to many amacrine cells, and their larger (than Parasol cells) dendritic fields. They report that there are about 30–40% as many Garland cells as Parasol cells which would agree with our figure of $\rho_y = 0.15*2$.

Three single cell electrophysiological studies indicate that M_y-cells are larger than M_x-cells by virtue of their larger receptive field size [17,31] and more rapid conduction velocities [31,16]. The behaviour of Y-like M-cells is quite different than their X-like partners with respect to light adaptation, such that Y-like cells preserve their temporal tuning and contrast sensitivity much better than X-cells as light levels fall from 1000 to 0.01Td [34]. More recently Smith III *et al.* [21] have demonstrated, through electrophysiological recordings from the LGN, that the larger members of both the P and M cell classes are more damaged by trauma induced glaucoma than the smaller members of these two cell classes. Unfortunately, low cell numbers and their use of relatively advanced glaucoma did not permit them to make a judgement as to whether M_y-cells are significantly more damaged that M_x-cells in early glaucoma. The fact that larger members of the M-cell pathway are differentially affected [21] suggests a different anatomical subset of M-cells.

4.7. Retinal gain control and motion perception

Aliasing is not a problem if the major task of Y-cells is to convey the state of retinal gain control to the brain. The signal governing retinal gain control, being essentially the local r.m.s. contrast, is unaffected by aliasing, spatial phase being of no import. Very briefly, the requisite contrast signal that gain control operates on seems to be computed by taking the spatial average of about 100 rectified bipolar cell inputs ([38] see also [97]). There also is a process of signal modification to provide the spatio-temporal tuning of the contrast sig-

nal to high speeds (i.e. low spatial and high temporal frequencies). This signal is then used to regulate M-cell gain [36] in primates, and X and Y cell gain in cats, [35,39,98] and is also added to the Y-cell response to give them their special character [5,6].

When computing the spectral power of a signal (the Fourier domain equivalent of averaging the square of the signal), aliasing poses no problems at all even for frequencies well beyond S_c, as long as the underlying sampling array is disordered [99,100]. In principle with certain *a priori* information it is even possible to accurately recover spatial phase information above S_c [49]. That is not what Y-cells appear to want to do with this information, however. Instead, they take the spatial sum of a large number of rectified signals and so the spatial phase information is largely destroyed except at very low spatial frequencies. Y-cells relay this contrast signal [6], and so too the state of retinal adaptation, to the brain.

Aliasing does pose problems for motion computation. With natural stimuli, being composed of every spatial frequency, the effect of aliasing will be to fold back energy above S_c into the band from 0 to S_c cpd and this energy will appear as noise. For example, in the central 2° the value of S_c is about 2 cpd (input frequencies) while individual M_y-cells within the 2.5° are reported as having a mean spatial resolution of 12 cpd or six times S_c [17]. This brings into question the suitability of M_y-cells as direct inputs to motion computation given that there is considerable power in retinal images in the band 2–12 cpd, and all of this will have its spatial phase information (positional information) degraded by aliasing, thus reducing the accuracy of calculation of motion in this band. Moreover, much of the power in the band 2–12 cpd will be aliased back into the band 0–2 cpd considerably degrading the signal to noise ratio even below S_c. Finally, while the ability of the linear response of Y-cells will be degraded by aliasing, the nonlinear response component has had much of its positional information degraded by spatial averaging.

These effects may explain why subjects can accurately identify drifting low contrast FD gratings while at the same time they cannot distinguish the direction of drift [11], even for spatial frequencies well below S_c. Loss of the ability to detect grating motion direction is typical of aliasing effects as seen for P-cell aliasing in the periphery [62,59,53].

Not only would Y-cells be bad at motion computation but they also appear not to be needed for cortical motion computation given that motion computation likely occurs *via* ON and OFF cells, which are either lagged or not lagged [72], as found in the X pathway [101,102]. Thus, spatial aliasing means that Y-cells may only participate indirectly in image motion computation by keeping the brain abreast of the rapidly changing retinal adaptive state which operates on a time scale of ≈ 15 ms [6]. This need for speed perhaps explains the need for rapid conduction in Y-cells. Strong Y-input to areas of the cortex associated with motion computation may have more to do with the necessity of disentangling rapid changes in ganglion cell gain from actual changes in contrast (see following section).

4.8. Spatial requirements for the operation of retinal gain control

A final consideration is that the process of retinal gain control may actually require a separate, coarse, array of cells. This conclusion comes about if one assumes that a primary role of M_y-cells is to convey the retinal gain control signal to the brain. It would seem foolhardy for the visual system to have the regions over which the contrast signal was computed to overlap in a haphazard fashion, so logic dictates that the Y-cells should have a fairly fixed inter-cell distance [103]. The most efficient detector packing strategy is a regular hexagonal array [43,47], but a disordered array, having some mean inter-detector difference $\pm$ sd, is a close approximation [67]. Such a moderately orderly array of course has a Yellott Ring spectrum [64,65] provided the standard deviation of the intercell distance is 15% or more of the mean distance, as occurs for primate photoreceptors from 0.5° retinal eccentricity outward [104].

A moderately orderly array of Y-cells would have implications for visual processing in striate cortex. If the M_y-cells represent about 20% of all M-cells then there are about 2–4 M_y-cells per cytochromeoxidase (CO) blob in V1 (e.g. [105]). The blob centred regions are the site of processing low spatial frequencies [106]. Any regulation of local contrast gain over large patches of the retina must have a huge impact on the interpretation of low spatial frequencies. That is to say the brain would have difficulty disambiguating actual changes in the contrast of low spatial frequencies from changes in contrast gain of the ganglion cell afferents where, as described above, the contrast control signal is computed as a spatial average, i.e. computed using low spatial frequencies as input. Therefore, given that blob centred regions could have to receive detailed and rapidly updated (≈ 15 ms) knowledge of retinal gain control from Y-cells, it is tempting to suggest that Y-cells synapse in the blobs where low spatial frequencies are processed. The region of visual space analysed by blob centred cortical units is slightly bigger than the typical receptive field area of M-cells (e.g. [105]Fig. 5) and is comparable to the area over which the contrast signal is computed [6,97], Fig. 6. Therefore a coarse, but fairly regular, array of M_y-cells would also serve the blob centred image analysis system well in supplying information about regulation of M-cell gain and its effects upon interpreting low spatial frequencies.

4.9. Conclusions

The present data provide good evidence that spatial aliasing effects can be observed for stimuli producing the spatial frequency doubled illusion. M_y-cells are good candidates for sources of the illusion. The predicted critical spatial frequency of M_y-cells S_c is a good match to the observed data at retinal eccentricities ranging from the fovea out to 40°, ρ_y being either 0.15 or 0.3 depending on whether ON- and OFF-centred cells act as 1 or 2 arrays. If there is a mechanism which chooses M_y-cells as the exclusive basis for motion computation when their (nonlinear) response is strong then this admits the possibility that the linear component of the M_y-cell response is used to compute motion and then ρ_y falls to about 0.05 near the lower limit reported [30]. The noise produced by aliasing may explain why direction selectivity is lost at contrasts well above the recognition threshold for FD patterns [11].

As long as the M_y-cells have a mean inter-cell distance greater than that of the M_x-cells then the first motion reversal is not affected by any second harmonic response component from the M_x-cells, even if the M_x-cells are somewhat nonlinear. Consideration of the efficient computation underlying the retinal gain control system [35,36], and also the ability of CO blob centred computational units in V1 to rapidly interpret low spatial frequency signals in the face of large scale changes in ganglion cell gain, both indicate that a separate coarse array of fast conducting Y-like cells is required.

Unlike motion computation, calculation of the contrast signal governing gain control is unaffected by spatial aliasing. It is possible that Y-cells could be used as inputs to motion computation for very high image velocities where only very low spatial frequencies (i.e. below S_c) would produce reasonable response modulation, thus minimising the effects of spatial aliasing. Animals making use of high image velocities might tend to use Y-cells more as inputs to image motion and take steps to reduce aliasing. This could for example explain why cats might have slightly denser Y-cell arrays than macaques.

Acknowledgements

The authors would like to thank T. Bossomaier, S.J. Galvin, S. Marcelja, A.W. Snyder and D.R.Williams for helpful discussions on the subject of sampling theory, and R.F. Mark and M.V. Srinivasan for reading versions of the manuscript and for their support. This work is dedicated to Dr. Lotte von Gavel who first used motion reversal to assess the density of an array of visual neurons [107].

References

[1] Kelly DH. Frequency doubling in visual responses. J Opt Soc Am 1966;56:1628–33.
[2] Tyler CW. Observations on spatial-frequency doubling. Perception 1974;3:81–6.
[3] Enroth-Cugell C, Robson JG. The contrast sensitivity of retinal ganglion cells of the cat. J Physiol 1966;187:517–22.
[4] Shapley RM, Perry VH. Cat and monkey retinal ganglion cells and their visual functional roles. Trends Neurosci 1986;9:229–35.
[5] Victor JD, Shapley RM. The nonlinear pathway of Y ganglion cells in the cat retina. J Gen Physiol 1979;74:671–89.
[6] Victor JD. The dynamics of the cat retinal Y cell subunit. J Physiol 1988;405:289–320.
[7] Kelly DH. Nonlinear visual responses to flickering sinusoidal gratings. J Opt Soc Am 1981;71:1051–5.
[8] Maddess T. Method and apparatus for use in diagnosis of glaucoma. Australian Patent 611, 585 (1989).
[9] Maddess T. Method and apparatus for use in diagnosis of glaucoma. USA Patent 5,065,767 (1991).
[10] Maddess T. Early detection of glaucoma. Australian patent application No PL 3130 (1994).
[11] Maddess T, Henry GH. Performance of nonlinear visual units in ocular hypertension and glaucoma. Clin Vis Sci 1992;7:371–83.
[12] Maddess T, Wine S, Dobinson J, Goldberg I, James AC. Clinical trials of psychophysical assessment of glaucoma using the frequency doubled illusion. Invest Ophthal Vis Sci 1997 (submitted).
[13] Maddess T, James AC, Wine S, and Goldberg I. Parallel PERG perimetry for glaucoma. Invest Ophthal Vis Sci 1997 (submitted).
[14] Johnson CA, Cello KE, Nelson-Quigg JM, Demirel S. Performance of frequency doubling perimetry for detecting various levels of glaucomatous field loss. Invest Ophthalmol Vis Sci 1997;38:200.
[15] Kaplan E, Shapley RM. X and y cells in the lateral geniculate nucleus of macaque monkeys. J Physiol 1982;330:125–43.
[16] Marrocco RT, McClurkin JW, Young RA. Spatial summation and conduction latency classification of cells of the lateral geniculate nucleus of macaques. J Neurosci 1982;2:1275–91.
[17] Blakemore C, Vital-Duran F. Organization and post-natal development of the monkey's lateral geniculate nucleus. J Physiol 1986;380:453–91.
[18] Quigley HA, Addicks EM, Green RW. Optic nerve damage in human glaucoma III Quantitative correlation of nerve fibre loss and visual field defect in glaucoma, ischaemic neuropathy, papilledema, and toxic neuropathy. Arch Ophthalmol 1982;100:135–46.
[19] Quigley HA, Dunkelburger GR, Green WR. Studies of retinal ganglion cell atrophy correlated with automated perimetry in human eyes with glaucoma. Am J Ophthalmol 1989;107:453–64.
[20] Glovinsky Y, Quigley HA, Pease ME. Foveal ganglion cell loss is size dependent in experimental glaucoma. Invest Ophthalmol Vis Res 1993;34:395–400.
[21] Smith III EL, Chino YM, Harwerth RS, Ridder III WH, Crawford MLJ, DeSantis L. Retinal inputs to the monkey's lateral geniculate nucleus in experimental glaucoma. Clin Vision Sci 1993;8:113–39.
[22] Johnson CA, Brandt JD, Khong AM, Adams AJ. Short-wavelength automated perimetry in low-, medium-, and high-risk ocular hypertensive eyes Initial baseline results. Arch Ophthalmol 1995;113:70–6.

[23] De Valois RL, Morgan H, Snodderly DM. Psychophysical studies of monkey De Valois vision-III Spatial luminance contrast sensitivity tests of macaque and human observers. Vis Res 1974;14:75–81.
[24] De Valois RL, Morgan H, Polson MC, Mead WR, Hull EM. Psychophysical studies of monkey vision-I Macaque luminosity and colour vision tests. Vis Res 1974;14:53–67.
[25] Harwerth RS, Boltz RL, Smith III EL. Psychophysical evidence for sustained and transient channels in the monkey visual system. Vis Res 1980;20:15.
[26] Stone J, Johnston E. The topography of primate retina: a study of the human, bushbaby, and new- and old-world monkeys. J Comp Neurol 1981;196:205.
[27] Curcio CA, Allen KA. Topography of ganglion cells in human retina. J Comp Neurol 1990;300:5–25.
[28] Dacey DM, Petersen MR. Dendritic field size and morphology of midget and parasol cells of the human retina. Proc Natl Acad Sci USA 1992;89:9666–71.
[29] Perry VH, Oehler R, Cowey A. Retinal ganglion cells that project to the dorsal lateral geniculate nucleus in the macaque monkey. Neuroscience 1984;12:1101–23.
[30] Derrington AM, Lennie P. Spatial and temporal contrast sensitivities of neurones in lateral geniculate nucleus of macaque. J Physiol 1984;357:219–40.
[31] Kaplan E, Shapley RM. The primate retina contains two types of ganglion cells, with high and low contrast sensitivity. Proc Natl Acad Sci USA 1986;83:2557–755.
[32] Crook JM, Lange-Maleki B, Lee BB, Valberg A. Visual resolution of macaque retinal ganglion cells. J Physiol 1988;396:205–24.
[33] Purpura K, Kaplan E, Shapley RM. Background light and the contrast gain of primate P and M retinal ganglion cells. Proc Natl Acad Sci USA 1988;85:4534–7.
[34] Purpura K, Trachina D, Kaplan E, Shapley RM. Light adaptation in the primate retina: analysis of changes in the gain and dynamics of monkey retinal ganglion cells. Vis Neurosci 1990;4:75–93.
[35] Shapley RM, Victor JD. The effect of contrast on the transfer properties of cat retinal ganglion cells. J Physiol 1978;285:275–98.
[36] Bernardete EA, Kaplan E, Knight BW. Contrast gain control in the primate retina: P cells are not X-like, some M cells are. Vis Neurosci 1992;8:483–6.
[37] Shapley RM, Victor JD. How the contrast gain control modifies the frequency responses of cat retinal ganglion cells. J Physiol 1981;318:161–79.
[38] Victor JD, Shapley RM. Receptive field mechanisms of cat X and Y retinal ganglion cells. J Gen Physiol 1979;74:257–98.
[39] Shapley RM, Victor JD. The effect of contrast on the non-linear response of the Y-cell. J Physiol 1980;302:535–47.
[40] James AC, Maddess T, Rouhan K, Bedford S, Snowball M. Evidence for My-cell involvement in the spatial frequency doubled illusion as revealed by a multiple region PERG for Glaucoma. J Opt Soc Am VSIA Tech Dig 1995;1:314–7.
[41] Bedford S, Maddess T, Rose KA, James AC. Correlations between observability of the spatial frequency doubled illusion and a multi-region PERG. Aus New Zealand J Ophthalmol 1997;25:91–3.
[42] Maddess T, Bedford S, James AC, Rose KA. A multiple frequency, multiple region pattern electroretinogram investigation of nonlinear retinal signals. Aus New Zealand J Ophthalmol 1997;25:94–7.
[43] Petersen DP, Middleton D. Sampling and reconstruction of wave-number-limited functions in n-dimentional euclidian spaces. Inf Control 1962;5:279–323.
[44] Bracewell RN. The Fourier Transform and its Applications. London: McGraw-Hill, 1978:189.
[45] Snyder AW, Laughlin SB, Stavenga DG. Information capacity of eyes. Vis Res 1977;17:1163–75.
[46] Snyder AW, Bossomaier TRJ, Hughes A. Optical image quality and the cone mosaic. Science 1986;231:499–501.
[47] Merserseau RM. The processing of hexagonally sampled two-dimensional signals. Proc IEEE 1979;67:930–49.
[48] Giesler WS, Hamilton DB. Sampling-theory analysis of spatial vision. J Opt Soc Am 1986;A3:62–70.
[49] Ruderman DL, Bialek W. Seeing beyond the Nyquist limit. Neural Comp 1992;4:682–90.
[50] Field DJ. Scale-invarience and self-similar 'wavelet' transforms: an analysis of natural scenes and mamalian visual systems. In: Farge M, Hunt JCR, Vassilicos JC, editors. Wavelets, Fractals, and Fourier Transforms. Oxford: Clarendon Press, 1993:151–93.
[51] Levitan B, Buchsbaum G. Signal sampling and propagation through multiple cell layers in the retina: modeling and analysis with multirate filtering. J Opt Soc Am 1993;A10:1463–80.
[52] Coletta NJ, Williams DR, Tiana CLM. Consequences of spatial sampling for human motion perception. Vis Res 1990;30:1631–48.
[53] Galvin SJ, Williams DR, Coletta NJ. The spatial grain of motion perception in human peripheral vision. Vis Res 1996;36:2251–9.
[54] Perry VH, Cowey A. The ganglion cell and cone distributions in the monkey's retina: implications for central magnification factors. Vis Res 1985;25:1795–810.
[55] Grünert U, Greferath U, Boycott BB, Wässle H. Parasol (Pα) ganglion-cells of the primate fovea: immunocytolchemical staining with antibodies against GABAA- receptors. Vis Res 1993;33:1–14.
[56] Thibos LN, Cheney FE, Walsh DJ. Retinal limits to the detection and resolution of gratings. J Opt Soc Am 1987;A4:1524–9.
[57] Smith RA, Cass PF. Aliasing in the parafovea with incoherent light. J Opt Soc Am 1987;A4:1530–4.
[58] Williams DR, Sekiguchi N, Brainard D. Color, contrast sesnitivity, and the cone mosaic. Proc Natl Acad Sci USA 1993;90:9770–7.
[59] Artal P, Derrington AM, Colombo E. Refraction, aliasing, and the absence of motion reversals in peripheral vision. Vis Res 1995;35:939–47.
[60] Galvin SJ, Williams DR. No aliasing at edges in normal viewing. Vis Res 1992;32:2251–9.
[61] Anderson SJ, Hess RF. Post-receptoral undersampling in normal human peripheral vision. Vis Res 1990;30:1507–15.
[62] Anderson SJ, Drasdo N, Thompson CM. Parvocellular neurons limit motion acuity in human peripheral vision. Proc R Soc London 1995;B261:129–38.
[63] Williams DR. Topography of the foveal cone mosaic in the living human eye. Vis Res 1988;28:434–54.
[64] Yellott JI. Spectral analysis of spatial sampling by photoreceptors: topological order prevents aliasing. Vis Res 1982;22:1205–10.
[65] Yellott JI. Spectral consequences of photorecptor sampling in the rhesus retina. Science 1983;221:382–5.
[66] Williams DR, Coletta NJ. Cone spacing and the visual resolution limit. J Opt Soc Am 1987;A8:1514–23.
[67] Coletta NJ, Williams DR. Psychophysical estimate of extrafoveal cone spacing. J Opt Soc Am 1987;A8:1503–13.
[68] Williams DR, Collier R. Consequences of spatial sampling by a human photoreceptor mosaic. Science 1983;221:385–7.
[69] Connolly M, Van Essen D. The representation of the visual field in parvicellular and magnicellular layers of the lateral geniculate nucleus. J Comp Neurol 1984;226:544–64.
[70] Van Essen D, Newsome WT, Maunsell JHR. The visual field representation in striate cortex of the macaque monkey: asym-

metries, anisotropies and individual variability. Vis Res 1984;24:429–48.
[71] Emerson RC, Citron MC, Vaughn WJ, Klein SA. Nonlinear directionally selective subunits in complex cells of cat striate cortex. J Neurophysiol 1987;58:33–65.
[72] Emerson RC, Bergen JR, Adelson EH. Directionally selective complex cells and the computation of motion energy in the cat visual cortex. Vis Res 1992;32:203–18.
[73] Wässle H, Levick WR, Cleland BG. The distribution of the alpha type of ganglion cells in the cat's retina. J Comp Neurol 1975;159:419–38.
[74] Lee BB, Martin PR, Valberg A. Nonlinear summation of M- and L-cone inputs to phasic retinal ganglion cells of the macaque. J Neurosci 1989;9:1433–42.
[75] van Doorn AJ, Koenderink JJ. The structure of the human motion detection system. IEEE Trans SMC 1983;13:916–22.
[76] Grünert U, Martin PR. Rod bipolar cells in the macaque monkey retina: immunoreactivity and connectivity. J Neurosci 1991;11:2742–58.
[77] Lennie P, Fairchild MD. Ganglion cell pathways for rod vision. Vis Res 1994;34:477–82.
[78] Lee BB, Smith VC, Pokorny J, Kremers J. Rod inputs to macaque ganglion cells and their temporal dynamics. Invest Ophthalmol Vis Sci 1996;37:689.
[79] Silveira LCL, Picanço-Diniz CW, Sampaio LFS, Oswaldo-Cruz E. Retinal ganglion cell distribution in the cebus monkey: a comparison with the cortical magnification factors. Vis Res 1989;29:1471–83.
[80] Wässle H, Grünert U, Röhrenbeck J, Boycott BB. Cortical magnification factor and the retinal ganglion cell density of the primate retina. Nature 1989;30:643–6.
[81] Schein SJ. Anatomy of macaque fovea and spatial densities of neurons in foveal representation. J Comp Neurol 1988;269:479–505.
[82] Chubb C, Sperling G. Two motion perception mechanisms revealed through distance driven reversal of apparent motion. Proc Natl Acad Sci USA 1989;86:2985–9.
[83] Maddess T and Severt L. Interaction of afterimages and motion reversal in drift-balanced stimuli. 1997 (in preparation).
[84] Anstis SM, Rogers BJ. Illusory reversal of visual depth and movement during changes of contrast. Vis Res 1975;15:957–61.
[85] Lu ZL, Sperling G. The functional architecture of human visual motion perception. Vis Res 1995;35:2697–722.
[86] Hochstein S, Shapley RM. Quantitative analysis of retinal ganglion cell classifications. J Physiol 1976;262:237–64.
[87] Geller AM, Sieving PA, Green DG. Effect on grating identification of sampling with degenerate arrays. J Opt Soc Am 1992;A9:472–7.
[88] Horton JC, Hedley-Whyte ET. Mapping of cytochrome oxidase patches and ocular dominance columns in human visual cortex. Philos Trans R Soc London 1984;B304:255–72.
[89] Merigan WH, Eskin TA. Spatio-temporal vision of macaques with severe loss of PB retinal ganglion cells. Vis Res 1986;26:1751–61.
[90] Merigan WH, Maunsell JHR. Macaque vision after magnicellular lateral geniculate lesions. Vis Neurosci 1990;5:347–52.
[91] Schiller PH, Logthetis NK, Charles ER. Role of color-opponent and broad-band channels in vision. Vis Neurosci 1990;5:321–46.
[92] McClurkin JW, Optican LM, Richmond BJ. Cortical feedback increases visual information transmitted by monkey parvocellular lateral geniculate nucleus neurons. Vis Neurosci 1994;11:601–17.
[93] Burr DC, Morrone MC, Ross J. Selective supression of the magnocellular visual pathway during saccdic eye movements. Nature 1994;371:511–3.
[94] Peichl L, Ott H, Boycott BB. Alpha ganglion cells in mamalian retinae. Proc R Soc London 1987;B231:169–97.
[95] Kaplan E, Lee BB, Shapley RM. New views of primate retinal function. Prog Retinal Res 1990;9:273–336.
[96] Sterling P, Calkins DJ, Kulg KJ, Schein SJ, Matsumoto Y. Parallel pathways from primate fovea. Invest Ophthalmol Vis Sci 1994;35:2001.
[97] Hochstein S, Shapley RM. Linear and nonlinear spatial subunits in Y cat retinal ganglion cells. J Physiol 1976;262:265–84.
[98] Victor JD. The dynamics of the cat retinal X cell centre. J Physiol 1987;386:219–46.
[99] Yen JL. On nonuniform sampling of bandwidth-limited signals. IRE Trans Circuit Theory 1956;3:251–7.
[100] Beutler FJ. Alias-free randomly timed sampling of stochastic processes. IEEE Trans Inform Theory 1970;16:147–52.
[101] Mastronarde DN. Two classes of single-input X-cells in cat lateral geniculate nucleus I Receptive field properties and classification of cells. J Neurophysiol 1987;57:357–80.
[102] Humphrey AL, Weller RE. Functionally distinct groups of X-cells in the lateral geniculate nucleus of the cat. J Comp Neurol 1988;268:429–47.
[103] Bossomaier TRJ, Snyder AW, Hughes A. Irregularity and aliasing: solution? Vis Res 1985;25:145–7.
[104] Hirsch J, Miller WH. Does cone positional disorder limit resolution? J Opt Soc Am 1987;A4:1481–92.
[105] Schein SJ, de Monasterio FM. Mapping of retinal and geniculate neurons onto striate cortex of macaque. J Neurosci 1987;7:996–1009.
[106] Tootell RBH, Silverman MS, Hamilton SL. Functional anatomy of macaque striate cortex. V. Spatial frequency. J Neurosci 1988;8:1610–24.
[107] von Gavel L. Die 'kritische streifenbreite' als mass der sehschärfe bei drosophila melanogaster. Z Vgl Physiol 1939;27:80–135.